Temporal limits of a rapidly swept Langmuir probe

Robert B. Lobbia and Alec D. Gallimore
Department of Aerospace Engineering, Plasmadynamics and Electric Propulsion Laboratory, The University of Michigan, Ann Arbor, Michigan 48109, USA

(Received 14 December 2009; accepted 20 May 2010; published online 7 July 2010)

The finite, electrostatically achievable, temporal resolution of plasma properties from a turbulent discharge is limited by an array of effects wherein the theory of Langmuir probes breaks down. Formulations for the particle transit time, sheath formation time, plasma-probe resonance, polarization current, sheath capacitance, stray capacitance, and mutual capacitance effects are all evaluated for time-resolved operation of a Langmuir probe. The resulting time scales serve to place a theoretical bound on the maximum rate of a rapidly swept Langmuir probe as analyzed with typical thin-sheath collisionless probe theory. For plasma typical to the plume of a Hall effect thruster [xenon plasma, $n_e=(1-1000)\times 10^{+15}$ m^{-3}, and $T_e=1-20$ eV], upper limits of 0.01–70 kHz are observed for a noncapacitive compensated Langmuir probe. With a high-speed dual Langmuir probe (HDLP) (a regular probe plus a null compensation probe), the upper probing frequency limits are increased to 0.04–11 MHz limited by sheath capacitance in the far and near field, and polarization effects for closer internal measurements. For a typical tokamak edge plasma (with HDLP), the thermally equilibrated hotter species (typically $T_e \approx T_i \approx 10$ to 20 eV) and lighter ions together lend higher limiting rates of ion transit, sheath formation, and sheath capacitance effects (in excess of 20 MHz), but the fully magnetized plasma complicates the collected probe current, limiting the allowable sweep rate to <1 MHz (for a magnetic field of 2 T). Thus we find that the upper rate of Langmuir probe sweeping is in the low megahertz range for both electric thruster and fusion plasma device diagnostics. © *2010 American Institute of Physics*.
[doi:10.1063/1.3449588]

I. INTRODUCTION

All plasmas exhibit transient fluctuations in their properties due to various electromagnetic interactions. For the interest of plasma based space propulsion, fusion devices, and other plasma systems, the largest magnitude oscillations occur at low frequencies of <1 MHz.[1–3] Time-resolved measurements of these plasma fluctuations are limited due to an emphasis of prior research on the time-averaged plasma properties using dc diagnostic techniques. However, there exists a growing interest in the temporally resolved nature of plasma discharge properties including: electron density $n_e(t)$, electron temperature $T_e(t)$ (or electron energy distribution function), and plasma potential $V_p(t)$. Anomalous transport in plasma thrusters and tokamaks alike is often attributed to turbulent plasma oscillations and low-frequency instabilities.[4–7] Cross-field electron flux leakage to the walls is one of the key containment challenges in modern magnetically confined fusion reactors and it also occurs in Hall effect thrusters (HETs) where it lowers thruster efficiency and increases the rate of erosion.

The original theory of electrostatic current collection by Mott-Smith and Langmuir[8] assumes equilibrium conditions for the sheath and particle flux or current measured at each probe bias. The most commonly listed temporal limitations of a single Langmuir probe are the times required to form a sheath and for charge carriers to traverse this sheath.[9,10] These limitations are common to all manner of the Langmuir probing (single, double, triple, fixed bias, or ramped bias), for all are based on electrostatic sheath flux equations.

Strong plasma oscillations are known to distort dc Langmuir probe measurements irrevocably—rendering their accuracy as questionable. Analytic flux formulations as well as empirical data incorporating temporally perturbed plasma and probe properties[11,12] show that dc probe measurements can experience greatly diminished accuracy for large fluctuations (with little adverse effects from small fluctuations).

These issues and others have imparted the need for time-resolved measurements that capture the fluctuating processes. While rf-compensated Langmuir probes and floating (or fixed-bias) double or triple probes can enable time-averaged and time-resolved measurements (without rapidly sweeping the probe bias), they require additional assumptions that can introduce their own problematic issues making them less than ideal for time-resolved measurements in unsteady plasma environments. Finally, the acquisition of direct back-to-back swept Langmuir probe time-resolved measurements—as opposed to phase-averaged measurements (e.g., enabled by the commercially available Hiden ESPion Langmuir probe) often made in pulsed plasmas[13]—is required for accurate and meaningful data from plasmas rich in turbulent character.

The following sections provide (for the first time) a nearly complete collection of the various temporal limits one might expect with a traditional swept Langmuir probe within the realm of thin-sheath collisionless theory. These limits are motivated with theory, numerical simulations, as well as empirical findings. The compiled formulas for the limiting probe sweep frequencies provide only order of magnitude

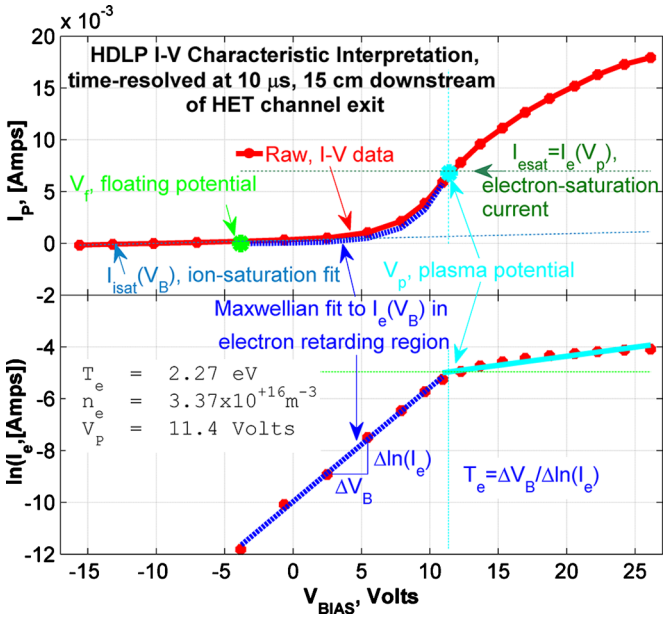

FIG. 1. (Color online) The important features of this HDLP *I-V* characteristic are labeled with the upper trace showing the raw probe current (after null probe correction) and bias voltage while the lower trace displays the effective electron current on a logarithmic scale. No averaging or smoothing has been applied to these time-resolved *I-V* data, demonstrating the effectiveness of the HDLP.

accurate upper bounds to the rates of plasma property acquisition achievable within the traditional electrostatic framework of Langmuir probe theory.

II. ELECTROSTATIC PROBE THEORY

A Langmuir probe is comprised of an exposed conductor (e.g., wire) immersed within a plasma. The theory of interpreting the data acquired from Langmuir probes is well established[9,14–18] and this same thin-sheath collisionless theory may also be applied to high-speed Langmuir probe experiments (within the limitations explored briefly in this article). The foundation of Langmuir probe theory is based on the probe current versus probe bias voltage (*I-V*) characteristic plot (see Fig. 1). In Fig. 1, the probe bias was linearly ramped (using a 50 kHz symmetric sawtooth waveform) between −15 and 25 V, during 10 μs, with simultaneous 2 MHz measurement of probe current and probe voltage (the raw *I-V* data plotted). For collisionless, magnetic-field-free, thin-sheath probe operation, the basic plasma properties of density, temperature, and potential are derived from the *Bohm sheath criterion*, a relation that balances the flux of charged particles to the conducting surface of the probe by use of the Poisson equation and other fundamental relations.

A. Simple Langmuir probe thin-sheath analysis

First, the floating potential (V_f) is taken as the probe bias (V_B, in volts from chamber ground) at which zero probe current is drawn from the plasma. Second, the electron current is determined as the difference between the measured probe current with a linear fit to the probe current (I_p) in the ion saturation region of the *I-V* trace (where $V_B \ll V_f$): $I_e(V_B)=I_p(V_B)-I_{\text{isat}}(V_B)=I_p(V_B)-[m_{\text{isat}}V_B+b_{\text{isat}}]$, applied at all biases. Next, the plasma potential (V_p) is taken as the bias with minimum electron impedance, found at $(dI_e/dV_B)_{\max}$. Then, a method of least squares is employed to determine the transition region ($V_f < V_B \leq V_p$) log-linear slope used for calculating the election temperature T_e, in eV,

$$T_e|_{\text{slope method}} = \left(\frac{d \ln I_e}{dV_B}\right)^{-1} = \frac{(V_2 - V_1)}{\ln\left(\frac{I_2}{I_1}\right)}. \tag{1}$$

$V_{1,2}$ and $I_{1,2}$ represent the probe bias voltage and electron current in the log-linear portion of the transition region. One may also compute the electron temperature by using the V_f and V_p directly with the electron mass m_e, and the ion mass m_i (Ref. 9),

$$T_e|_{\text{potential method}} = (V_p - V_f)\frac{\ln}{\left(\sqrt{\frac{m_i}{2\pi m_e}}\right)}. \tag{2}$$

This and the preceding equations rely on assuming a Maxwellian electron velocity distribution. For cases where the plasma may possess a non-Maxwellian distribution one may define an effective electron temperature by partially integrating the first part of Eq. (1) (Refs. 18 and 19),

$$T_e|_{\text{effective}} = \frac{1}{I_{\text{esat}}}\int_{V_f}^{V_p} I_e(V_B)dV_B. \tag{3}$$

For a truly Maxwellian plasma, the prior three equations yield equivalent electron temperatures. Figure 2 compares these methods with time-resolved high-speed dual Langmuir probe (HDLP) data 10 cm downstream from a 200 V, 2 A Hall thruster discharge (on the axis of the discharge channel). This same thruster discharge was used to collect the data in Fig. 1. Ion and electron densities (n_i and n_e) are then estimated with the following formulas:[9]

$$I_{\text{isat}} = -\exp\left(-\frac{1}{2}\right) e n_i A_p \sqrt{\frac{eT_e}{m_i}},$$
$$I_{\text{esat}} = e n_e A_p \sqrt{\frac{eT_e}{2\pi n_e}}. \tag{4}$$

The parameter A_p represents the exposed area of the Langmuir probe with e as the electron charge (all SI units, except electron temperature in eV). The electron saturation current is measured as the current, which the probe absorbs with a sufficiently high ion-repelling positive-bias potential, here taken as $I_{\text{esat}}=I_e(V_B=V_P)$ (shown in Fig. 1). The ion saturation current is the current measured when the probe is at a large negative bias that repels all electrons. For I_{isat}, the sheath area is typically used in place of the probe area but to avoid an inevitable iteration process and to keep the analysis simple, the probe area is always used here. As the Debye length (proportional to the sheath size) approaches the probe size (and thin sheaths no longer persist), the use of probe area in Eq. (4) can give rise to significant errors in the computation of ion density n_i. For this reason (and others), HDLP data presented will make use only of the electron density as determined using the electron saturation current.

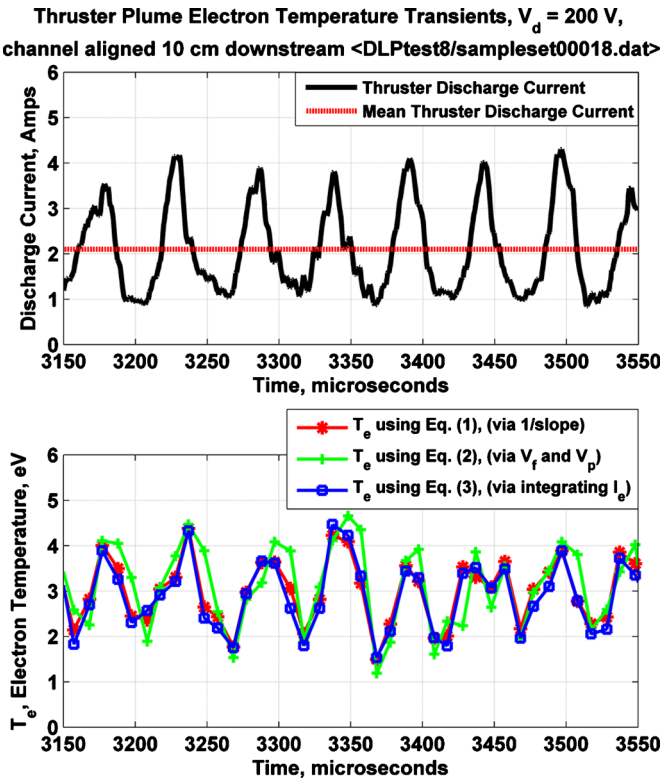

FIG. 2. (Color online) A comparison of time-resolved electron temperature formulations using Eqs. (1)–(3). Temperature fluctuations (at about 19 kHz) appear nearly in-phase (and close in relative magnitude) with simultaneously sampled thruster discharge current fluctuations. Time-resolved electron density and plasma potential data (not shown) acquired at this position also exhibit qualitatively similar fluctuations [with $n_e(t)$ following the thruster discharge current at the expected ion transit time].

Theoretically, a probe biased at the local plasma potential is sheathless, and a thin sheath is less requisite when density is computed using I_{esat}. However, at the plasma potential the larger probe currents may perturb the local plasma properties.

B. Temporal resolution limits

The ability for the plasma to properly respond to a rapidly changing probe bias is now shown to be limited by at least six temporally constraining issues: (1) sheath transit time, (2) sheath formation time, (3) plasma resonance, (4) polarization drift, (5a) sheath capacitance, (5b) stray capacitance, and (5c) mutual capacitance [(5c) for the HDLP only)].

1. Sheath transit time

The first limiting time scale examined is the transit time a particle requires to traverse the entire sheath surrounding a Langmuir probe immersed in a plasma. A few basic assumptions are needed including planar sheath with dimension on the order of three Debye lengths ($x_s = s\lambda_D = 3\lambda_D$), zero electric field at sheath edge, parabolic spatial potential variation inside sheath $V(x) = V_p - V_p x^2/x_s^2$, and initial particle velocity at sheath edge (directed toward probe) as the mean (Maxwellian) thermal speed. Integration then yields the following set of transit times for ions (τ_i) and electrons (τ_e), respectively,[9]

$$\tau_i = \sqrt{\frac{s^2 T_e}{8\pi^2 V_p}\left(\frac{m_i \in_o}{n_i e^2}\right)\ln\left(\frac{8V_p}{T_i}\right)} \approx 0.56 f_{pi}^{-1},$$
$$\tau_e = \sqrt{\frac{s^2 T_e}{8\pi^2 V_p}\left(\frac{m_e \in_o}{n_e e^2}\right)\ln\left(\frac{8V_p}{T_e}\right)} \approx 0.48 f_{pe}^{-1}. \quad (5)$$

This equation introduces, $\in_o$, the permittivity of free space in F/m, and uses the electron and ion temperatures in eV. The two frequencies included are the ion plasma frequency, f_{pi}, and the electron plasma frequency, f_{pe}. This result shows that ions and electrons traverse the sheath in about one-half of a fundamental plasma oscillation cycle. Most common laboratory plasmas possess electron plasma frequencies in excess of 1 GHz so the collection of electron current during the electron retarding portion of the Langmuir probe *I-V* characteristic (used to determine T_e) as well as the electron saturation current collection will be relatively uncorrupted for probe sweep rates as brief as a few nanoseconds (neglecting other effects). The ions, however, exhibit slower travel across the thin sheaths under analysis, requiring a time that is longer by the factor $\sqrt{m_i/m_e}$ to move from sheath edge to probe surface. In this way, the ion current collected may be underpredicted in the ion saturation region for situations, in which the probe bias sweep rate is on the order of the ion plasma frequency (typically exceeding a few megahertz).

2. Complete sheath formation

The time required to form a fully steady-state equilibrium sheath is examined next. As the Langmuir probe bias is adjusted (e.g., linearly ramped sawtooth sweep), adherence to the traditional thin-sheath Langmuir probe theory of current collection depends critically on the capability of the sheath to change its size and species composition at a rate faster than the rate of probe bias adjustment. While at first glance it may appear that the electron sheath formed at large positive probe bias is able to adjust itself quite rapidly (in a few nanoseconds) due to the large thermal electron velocities, Chen[14] argued that the ions presented initially in the formation of the electron sheath must still be displaced before sheath equilibrium is attained. Indeed, numerical studies[20–22] of the sheath response about rapidly adjusted surface potentials suggest a few (up to ten) ion plasma cycles are required to achieve an equilibrium sheath size,

$$\tau_{\text{sheath form,simulated}} \approx 10 f_{pi}^{-1}. \quad (6)$$

Integration of the continuity equation with an unsteady sheath size defined using the Child–Langmuir sheath equation yields the following theoretical estimate for the time to attain a steady-state sheath size:[23]

$$\tau_{\text{sheath form,Child–Langmuir}} \approx \frac{2^{1/4}}{9\pi}\left(\frac{V_p - V_B}{T_e}\right)^{3/4} f_{pi}^{-1}, \quad V_B \ll V_p. \tag{7}$$

Yet this formulation and the preceding formulation are only accurate for very high-voltage ion sheaths typical of ion implantation devices.

Directly exposed electrode experimental measurements of transient sheath formation are confounded by the presence of the many time-dependent effects herein discussed (e.g., transit, sheath capacitance, etc.). Even so, experiments carried out by Oskam *et al.*[24] suggested that for higher pressure ($\sim$1 torr) discharges, the charged carrier motion is ion mobility controlled (μ_i), such that the time for charge carrier redistribution is approximately[9]

$$\tau_{\text{sheath form,ion mobility controlled}} \approx \frac{\in_o}{en_i\mu_i}. \tag{8}$$

Next considered is a modified approach inspired by Loeb's examination of the sheath formation rate,[25] which applies an estimate using the time required for charged-particle thermal fluxes to replenish the volume occupied by the probe (plus sheath),

$$\tau_{\text{sheath form,thermal}} \approx \frac{4V_{\text{sheath volume}}}{(A_{\text{sheath area}}U_{\text{ion velocity}})} \approx 2(r_p + \lambda_D)/\sqrt{eT_e/m_i}. \tag{9}$$

Finally, one last consideration to our sheath formation time scale is the effect of plasma flow. While the flow speed, U_∞, remains well below the thermal speeds for the individual species, the effects on sheath formation will be minimal.[26,27] Once the plasma flow or drifting speed is on the order of (or exceeds) the thermal speeds, one might expect from Eq. (9) that the time for sheath formation could be significantly reduced for large effective $U_{\text{ion velocity}}$. The estimated average plasma drift velocity at the downstream HET plume locations in Figs. 1 and 2 is about 10 km/s—a speed that is several times the estimated Bohm speed. To incorporate this effect, here it is proposed to use the flow drift speed as $U_{\text{ion velocity}}$ in a manner similar to Eq. (9), to obtain (for a cylindrical probe axis perpendicular to the flow) a sheath formation time that includes flow effects,

$$\tau_{\text{sheath form,flow}} \approx 2(r_p + \lambda_D)/U_\infty. \tag{10}$$

It should be noted that for large flow speeds ($U_\infty >$ Bohm speed) such as the mesothermal plasma of most electric thrusters, a sizable (often dominant since the wake region downstream appears to absorb very little current[28]) "ram" current ion flux is directed to the probe.[27,29] Adapting this flux to include probe bias dependence (that is negligible for $U_\infty \gg U_{\text{Bohm}}$) obtains $I_{i,\text{ram}} = -A_\perp en_i[U_\infty \pm \sqrt{(e|V_p - V_B|)/m_i}] \approx -2r_pL_pen_iU_\infty$. This expression is only valid for wakeless thin sheaths with $e|V_p - V_B| \ll \frac{1}{2}m_iU_\infty^2$ and, in general form, shows an increase (+) in ion current $\propto |V_p - V_B|^{1/2}$ for $V_B < V_p$ and a decrease (−) for $V_B > V_p$. The probe area perpendicular to the flow vector, $A_\perp$, has been evaluated for a flow-transverse-oriented cylindrical probe of length, L_p, and radius, r_p. The flow velocity at which this current flux matches the (non-drifting) probe ion saturation current is $U_\infty|_{\text{Iisat=}Ii,\text{ram}} \approx \pi\exp(-1/2)\sqrt{eT_e/m_i} \approx 2U_{\text{Bohm}}$. Thus, in general, to minimize this extra current it is preferred to operate a Langmuir probe in regions where the plasma drifting speed is much less than the Bohm speed ($U_\infty \ll 2U_{\text{Bohm}}$). Yet, it is often out of the experimentalist's control to ensure low flow velocities, and in this case one can (ignoring sheath effects) correct the collected plasma current by simply subtracting out the extra ion flux that reaches the probe, $I_{i,\text{ram}}$ (at all biases below the ion-beam energy, $E_{i,\text{beam}}$).[30] Even without the preceding correction, the electron retarding region (and the electron saturation region in some cases) is largely unaffected by sub- or supersonic ion drifts (while the electron thermal speed $\gg U_\infty$).[31] For subsonic ion drifts ($U_\infty < U_{\text{Bohm}}$, predominant in the *isothermal* plasma of fusion devices)[32] the ion current collected by a thin-sheath Langmuir probe is largely unaffected since the flow merely alters the size of the presheath (shown to disappear[26] as $M_\infty = U_\infty/U_{\text{Bohm}} \to 1$) and that of the Debye sheath, and neither sheath size affects thin-sheath current collection theory. Finally, it is observed that by computing I_e from subtraction of a linear fit to the ion saturation current (as in Sec. II A), the extra ram current is conveniently removed (without knowledge of U_∞) as well, but interpretation of I_{isat} must be adjusted, perhaps by using the general form of $I_{i,\text{ram}}(V_B)$, when computing the ion density.

3. Resonance effects

Plasma resonant probes rely on constructive interference between probe potential oscillations and natural plasma oscillations. At a frequency, f_{resonant}, near the electron plasma frequency, f_{pe}, resonance occurs, and a sizable increase in the dc collected plasma current occurs, ΔI_{dc}. The theoretical resonant frequency for a spherical electrode is[9] $f_{\text{resonant}} \approx f_{pe}[1 + r_p/(5\lambda_D)]^{-2}$. To avoid such resonance effects it is necessary to operate Langmuir probes at sweep rates significantly below the resonant frequency, f_{resonant}. The nonlinear nature of this extra plasma current (ΔI_{dc}) leaves no immediate means to accurately remove this extra current (as one could with extra flowing plasma current in the previous section). Since the electron plasma frequency is typically quite large (>1 GHz) this resonance is unlikely to be comparable to the rate of probe sweeping. Resonance near the ion plasma frequency does also exist, but the extra current is considerably less pronounced[9] and the magnitude of extra current is rather small, thus ion plasma frequency resonance effects may usually be neglected.

4. Magnetic-field effects

Magnetic fields play crucial roles in many plasma systems including the ionizing closed drift in HETs and plasma confinement in tokamaks. In general, the effect of a strong magnetic field upon the collection of current by a Langmuir probe involves the restriction of charged carrier flux to the probe by limited cross magnetic field line charge motion. Now, when the oscillating potential of a rapidly swept

Langmuir probe is thrown into a magnetic field, one generates an additional drift current collected by the probe. Theoretically, this extra polarization drift current is evaluated as[33,34]

$$I_{\mathrm{pol}} = \frac{A_p(m_i n_i + m_e n_e)}{-B^2}\frac{dE_\perp}{dt}, \tag{11}$$

$$I_{\mathrm{pol}}|_{V_B=V_f} \approx \frac{A_p n_o}{-\lambda_D B_\parallel^2}\left\{\frac{Z_e m_e}{\left(\frac{m_i}{2\pi m_e}\right)^{-1/2}} + \frac{Z_i m_i \exp\left(-\frac{1}{2}\right)}{\left[1+\ln\left(\frac{m_i}{2\pi m_e}\right)^{1/2}\right]}\right\}\frac{dV_B}{dt},$$

where the magnetic field strength $B_\parallel$ is taken as the component parallel to the axis of a cylindrical Langmuir probe; for a magnetic field perpendicular to the probe, the polarization currents on each side of the probe nullify each other. The second line of Eq. (11) is evaluated at the surface of the probe where the electric field (using Poisson's equation with the Boltzmann relation) and thus dE/dt is non-negligible: $(dE/dt)_{\mathrm{surf}} \approx \lambda_D^{-1} dV_B/dt$. Also, a bias near the plasma floating potential is chosen (since the relative effect of the polarization current is greatest when $I_{\mathrm{probe}} \approx 0$) to compute the probe-surface electron and ion densities in terms of the bulk plasma density n_o. Lastly, in Eq. (11), the degree of magnetization, $Z_{e,i}$, terms are both zero in the majority of a HET plume (including the data in Figs. 1 and 2) since $r_{Li,e}/r_p \gg 1$ (however, very close to the thruster the electrons become magnetized as the electron Larmor radius approaches the probe radius, $r_{Le} \approx r_p$). While the lack of ion magnetization in HET discharges causes the usually dominant ion polarization drift (often termed the "inertial drift") to disappear, the fully magnetized plasma in a tokamak $Z_{e,i}=1$ is instead dominated by the ion polarization drift since $m_i \gg m_e$.

5. Capacitive effects

Swift variations of a conductor potential generate leakage or displacement currents that follow the basic capacitance relation: $I = C \times dV/dt$. For the rapidly swept HDLP data presented, the large voltages and short microsecond time scales lead to milliamperes of leakage current ($\gg I_{\mathrm{isat}}$) from tiny (from 1 pF to 1 nF) environmental capacitances. For a Langmuir probe, capacitive sources include probe-sheath capacitance to the plasma, probe-line stray capacitance to a ground plane, and probe-line mutual capacitance between neighboring conductors (see Fig. 3).

C. Sheath capacitance

Experiments by Oskam *et al.*[24,35] in the early 1960s showed large sheath capacitive displacement currents ($I_{\mathrm{displacement}} = C_{\mathrm{sheath}} dV_B/dt$) drawn by a special Langmuir probe for high-pressure (~1 torr) neon and helium discharges. The conclusions of these works showed that the

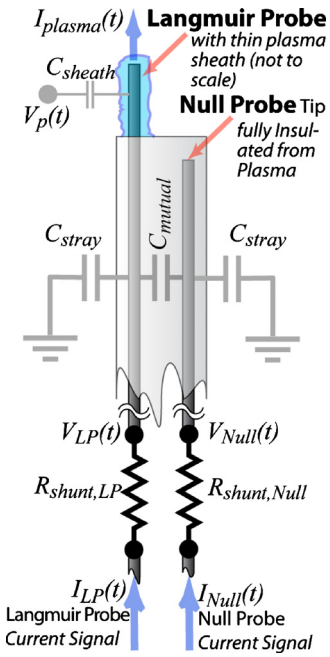

FIG. 3. (Color online) Schematic of HDLP configuration including effective sheath, stray, and mutual capacitances. The Langmuir and null probes maintain very close proximity to each other (<10 mm separation for over 10 m of cabling). The current measurement shunts are placed near the probe bias amplifier.

effective sheath capacitance was greatest at higher plasma densities in agreement with reduced Debye lengths. This finding makes sense, and in a separate work by Crawford and Grard,[36] the sheath capacitance about a planar Langmuir probe was estimated (using two different methods including Child–Langmuir sheath thickness and a Boltzmann treatment) at the floating potential as

$$C_{\mathrm{sheath}} \approx \alpha \frac{\in_o A_{\mathrm{probe}}}{\lambda_D}. \tag{12}$$

The nondimensional factor, α, ranges from about 0.1 to 1 according to both theoretical treatments and experimental data, so a value of 0.5 is taken as a conservative estimate since the Child–Langmuir sheath thickness is known to underpredict the true sheath size (especially in collisionless plasmas with probe biases only a few factors of T_e below V_p).[37] In any case, within an order of magnitude, the sheath capacitance in Eq. (12) provides a rough estimate of the capacitive effect of the plasma sheath about a Langmuir probe. For many probe/plasma measurements, this capacitance is on the order of a few picofarads—a sufficiently small capacitance that can generally be ignored as a sweep rate limiter in many cases.

D. Stray capacitance

Often referred to as parasitic capacitance, stray capacitance is formed between a conductor and its environment. Even a suspended bare wire in vacuum meters away from any conductive surface possesses nearly 10 pF/m of length. Stray capacitance exists for every conductor, and while methods exist to minimize the incurred displacement cur-

rents, such capacitance cannot be directly eliminated. Estimating stray capacitance from geometry alone is nonpractical thus a direct measurement of the stray capacitance for a given configuration is often required. A measurement of the displacement (or leakage) current present from stray capacitance in a Langmuir probe setup is possible by simply measuring the current voltage characteristic (I-V curve) without any plasma present. For a symmetric triangular sawtooth bias voltage signal the dV/dt is constant during each sweep so that the measured current during each sweep is also constant with either $I_{\text{disp}}>0$ for $dV_B/dt>0$ or $I_{\text{disp}}<0$ for $dV_B/dt<0$. The alternative HDLP approach of simultaneously sweeping two closely positioned probes, a Langmuir and a null probe, allows direct measurement of the stray (and some of the sheath) capacitively generated displacement current. Direct numerical subtraction of the two synchronously measured currents yields the true plasma current (ignoring mutual capacitance),

$$I_{\text{plasma}}(t) = I_{\text{LP}}(t) - I_{\text{null}}(t). \tag{13}$$

The dual probe configuration employed here is that drawn in Fig. 3. The preceding removal of displacement current also serves to remove any extraneous noise electromagnetic interference pickup by the probes since their close proximity ensures identical pickup in each probe—which is identically canceled upon subtraction. It is quite easy to produce leakage currents that exceed the ion saturation current. For example, a moderate 1 nF of stray capacitance (equivalent capacitance from 10 m of common coaxial cable) and a 100 V of bias sweeping over 1 μs produces 100 mA of displacement current,

$$I_{\text{leak}} = C_{\text{stray}}\frac{dV_B}{dt} = (1\times 10^{-9}\ \text{F})\times\left(\frac{100\ \text{V}}{1\times 10^{-6}\ \text{s}}\right) = 100\ \text{mA}. \tag{14}$$

This is a large amount of current for most small Langmuir probes, and while its distributed nature will prevent the probe from melting, it may well saturate the probe bias amplifier or the current measurement circuitry. Even with the ability to correct for stray currents, it is important to use low-capacitance wiring (e.g., avoiding shielded wires such as coaxial cable) and low-capacitance feedthroughs in order to keep the displacement currents to a minimum when sweeping rapidly.

E. Mutual capacitance

The addition of a null probe (or shielded wiring) may induce mutually capacitive current flow between the separate conductors (C_{mutual} in Fig. 3). However, since the dual probe configuration involves biasing both probes in an identical manner, the voltage between the probes is zero and thus the current from mutual capacitance is also zero. Yet, in the common configuration using shunt based probe current measurement, the Langmuir probe may be drawing significantly more current than the null probe, which corresponds to a larger voltage drop across the sensing resistor and hence a voltage difference between the probe biases thereby setting up a mutual capacitive current. This effect can be minimized by avoiding shunts (and using split-core Hall current probes) or by using very small shunt resistors. Alternatively, the effect may be canceled out by adding the Langmuir probe and null probe current signals or by adding some terms to Eq. (13),

$$I_{\text{plasma}}(t)^* = I_{\text{LP}}(t) + I_{\text{null}}(t) - C_{\text{stray}}\frac{d}{dt}(V_{\text{null}} + V_{\text{LP}}),$$
$$I_{\text{plasma}}(t)^* = I_{\text{LP}}(t) - I_{\text{null}}(t) + (2C_m + C_{\text{stray}})\frac{d}{dt}(V_{\text{null}} - V_{\text{LP}}). \tag{15}$$

These expressions cancel mutual capacitance (C_m) with estimations of stray and mutual capacitances and with numerically computed derivatives (capacitance estimation is possible in the ion saturation portion of the I-V characteristic where the Langmuir and null probe currents are closely matched). Generally, mutual capacitance is smaller than the stray capacitance and, in addition, the interprobe dV/dt is smaller for the mutual capacitance current, thus in many cases mutual capacitive effects may be neglected altogether.

F. Alternative capacitance cancellation technique

Another method of rapid sweeping, nearly as effective as the HDLP approach, is to employ double-shielded cabling (e.g., triaxial cabling). In this configuration (common with space plasma measurements)[38] the inner shield (or guard) and the central conductor are both simultaneously biased while a shunt resistor in line with the center conductor provides a measure of current with virtually zero stray line capacitive current. In theory, this should provide better capacitance correction than the HDLP, yet in practice the rather large capacitance (1 nF is typical) between the guard and outer shields can destabilize or saturate many bias amplifiers. Also, extra attention is needed to eliminate or minimize capacitive sources such as feedthroughs (a triaxial vacuum feedthrough is required) and measurement circuitry since this configuration does not allow for measuring stray capacitance from sources other than the probe transmission line.

1. Summary of temporal sweeping limits

The discussion in the preceding sections is now distilled into a set of effective frequencies at which the particular effect occurs or creates a current equivalent to I_{isat},

$$f_{\text{transit}} \approx 2f_{pi},$$
$$f_{\text{sheath formation}} \approx \pi\left(3+\frac{r_p}{\lambda_D}\right)^{-1} M_\infty f_{pi},$$
$$f_{\text{resonant}} \approx \left(1+\frac{r_p}{5\lambda_D}\right)^{-2}\sqrt{\frac{m_i}{m_e}}f_{pi},$$

TABLE I. Tabulation of Langmuir probe frequency sweep limits for typical HET and tokamak conditions [near-wall and scrape off layer (SOL) conditions are common Langmuir probe-able regions while the core is too hot to probe but included to show continued trends].

Typical case	n_e (m^{-3})	T_e (eV)	B (T)	f_{pi} (MHz)	f_{transit} (MHz)	$f_{\text{sheath form}}$ (MHz)	f_{resonant} (MHz)	f_{polariz} (MHz)	$f_{\text{sheath cap}}$ (MHz)	$f_{\text{stray cap}}$ (MHz)	$f_{\text{mut cap}}$ (MHz)
$\text{HET}_{\text{far-field}}$	10^{+15}	1	2×10^{-4}	0.6	1.2	7.1	140	∞	0.04	1×10^{-5}	3×10^{-4}
$\text{HET}_{\text{near-field}}$	10^{+16}	5	0.001	1.8	3.7	8.6	350	∞	0.7	3×10^{-4}	0.01
$\text{HET}_{\text{very-near-field}}$	10^{+17}	10	0.01	5.8	11.6	11.8	516	4.2	4.4	0.005	0.11
$\text{HET}_{\text{internal}}$	10^{+18}	20	0.02	18.3	36.6	14.3	559	10.6	28	0.07	1.5
$\text{TOKAMAK}_{\text{wall}}$	10^{+19}	10	2	467	934	21	136	0.8	356	3.7	87
$\text{TOKAMAK}_{\text{SOL}}$	10^{+20}	20	2	1476	2952	30	93	0.5	2250	52	1224
$\text{TOKAMAK}_{\text{core}}$	10^{+21}	$2\times10^{+3}$	2	4668	9336	813	17 677	168	$7\times10^{+6}$	$2\times10^{+4}$	$4\times10^{+5}$

$$f_{\text{polarization}} \approx \frac{2\pi \exp\left(-\frac{1}{2}\right) eB_{\parallel}^2 \lambda_D^2 \Delta V_B^{-1}}{Z_e m_e \sqrt{\frac{m_i}{2\pi n_e}} + \frac{Z_i m_i \exp\left(-\frac{1}{2}\right)}{\sqrt{1+\ln\left(\frac{m_i}{2\pi m_e}\right)}}} f_{pi}, \quad (16)$$

$$f_{\text{sheath capacitance}} = 4\pi \exp\left(-\frac{1}{2}\right)\left(\frac{T_e}{\Delta V_B}\right) f_{pi},$$

$$f_{\text{stray capacitance}} = 2\pi \exp\left(-\frac{1}{2}\right)\left(\frac{A_p \in_o}{C_{\text{stray}} \lambda_D}\right)\left(\frac{T_e}{\Delta V_B}\right) f_{pi},$$

$$f_{\text{mutual capacitance}} = 2\pi \exp\left(-\frac{1}{2}\right)\left(\frac{A_p \in_o}{C_{\text{mut}} \lambda_D}\right)\left(\frac{T_e}{\Delta V_B}\right) f_{pi}.$$

Simplified by using the Debye length and the ion plasma frequency [$2\pi f_{pi} \equiv \sqrt{n_i e^2/(m_i \in_o)}$], this collection of sweep rate limits is quite similar, although more complete, to an analysis by Chiodini *et al.*[39] The ion Mach number, M_∞, is included in the sheath formation frequency to incorporate the effect of a flowing plasma (for nondrifting plasmas with $U_\infty \leq U_{\text{Bohm}}$, set $M_\infty = 1$ as ensured by the presheath). Also, the bias sweep rate terms in Eq. (16) have been evaluated for symmetric sawtooth probe bias signals using $(dV_B/dt)_{\max} = \Delta V_B f_{\max}$, with $f_{\max}^{-1}$ equal to the time taken to slew ΔV_B, the peak-to-peak amplitude of a single probe bias sweep; for a sinusoidal sweep $(dV_{B,\sin}/dt)_{\max} = \pi \Delta V_B f_{\max}$. In maintaining a probe sweep rate much lower than each of these limiting frequencies, one shall remain within the realm of conventional electrostatic Langmuir probe theory,

$$f_{\text{sweep}} \ll \begin{cases} f_{\text{transit}}, f_{\text{sheath formation}}, f_{\text{resonant}} \\ f_{\text{polarization}}, f_{\text{sheath capacitance}} \\ f_{\text{stray capacitance}}, f_{\text{mutual capacitance}}. \end{cases} \quad (17)$$

The first three limiting frequencies (transit, sheath formation, and resonant) are rigid requirements that cannot be avoided. The later four limits (polarization and capacitive) are less restricting (e.g., with a HDLP, the stray capacitive limit is revoked) since the probe sweep rate may approach (or even exceed to some extent) these frequencies by only incurring minimal *I-V* trace distortion manifested primarily in the loss of I_{isat} and V_f accuracy. In some cases this *I-V* distortion can be removed; for example, by sweeping faster than the plasma variations (such that T_e and n_e are slowly varying constants) an estimate of the plasma capacitance *at each probe bias* is possible by comparing two consecutive (and opposite sign) bias sweeps.

For plasma conditions typical of a Hall thruster plume and tokamak edge region, the computed tabulation of frequency limitations is presented in Table I. A single Langmuir probe without capacitance compensation is unsweepable at and beyond about 0.01–70 kHz for typical HET plasma conditions. Sweeping a single probe this fast will generate stray capacitive current to the probe on the order of the ion saturation current, which will distort the *I-V* characteristic. However, the addition of a null probe (using a HDLP) increases the maximum rate of sweeping by orders of magnitude, enabling sweep rates for both HETs and tokamaks in the low-megahertz range.

In Table I, stray and mutual capacitances are calculated for 10 m of coaxial cabling and parallel ribbon cabling (1 cm conductor-separation 0.5 mm wire outside diameter), respectively, with $\Delta V_B = 100$ V and $A_p = 16$ mm^2. Far- and near-field HET plasmas are completely nonmagnetized, while only the electrons are magnetized for very-near-field and internal cases. The usage of a HDLP removes the effect of stray capacitance (and mutual capacitance with proper setup) that otherwise limits the bias sweep rate to low-kilohertz values. For a HDLP in the far and near fields of a HET, the temporally limiting feature is actually the probe-sheath capacitance, which limits the sweep rate to about 0.04–1 MHz. In very-near-field and internal HET measurements, the magnetization of the electrons introduces an electron-only polarization drift that instead serves to limit the HDLP sweep rate to 4–11 MHz. For typical tokamak edge conditions, the lighter species along with the hotter and denser thermalized plasma suggest that one could sweep a HDLP at rates >20 MHz, yet the fully magnetized plasma near the probe is affected with a large polarization drift current that exceeds the ion saturation current at sweep rates $>500-800$ kHz.

III. CONCLUSIONS

An exploration of seven temporally limiting features inherent to electrostatic Langmuir probe thin-sheath theory has significantly refined the estimate for the smallest-attainable temporal resolution beyond the often quoted limit of f_{pi}^{-1}.

While the inverse ion plasma frequency is indeed a fundamental limiting time scale, the additional analysis herein detailed shows swept-probe capacitance effects distort the *I-V* characteristic at frequencies orders of magnitude below f_{pi}. However, use of a HDLP governed by relatively simple electrostatic thin-sheath theory enables one to sample the plasma properties of electron temperature, electron density, and plasma potential at near-microsecond time scales for a variety of HET and tokamak plasma conditions. HET plume measurements with a 100 kHz HDLP show dramatic plasma fluctuations characteristic of a natural HET ionization instability (the so-called thruster breathing mode) and these results and the HDLP are detailed in a separate paper,[40] demonstrating the viability of the diagnostic and the limiting frequencies thus examined.

[1] E. Y. Choueiri, Phys. Plasmas **8**, 1411 (2001).
[2] H. De Kluiver, C. J. Barth, and A. J. H. Donne, Plasma Phys. Controlled Fusion **30**, 699 (1988).
[3] G. Y. Antar, G. Counsell, Y. Yu, B. Labombard, and P. Devynck, Phys. Plasmas **10**, 419 (2003).
[4] G. S. Janes and R. S. Lowder, Phys. Fluids **9**, 1115 (1966).
[5] C. Boniface, L. Garrigues, G. J. M. Hagelaar, J. P. Boeuf, D. Gawron, and S. Mazouffre, Appl. Phys. Lett. **89**, 161503 (2006).
[6] J. W. Connor, A. Fasoli, C. Hidalgo, A. Kirk, V. Naulin, A. G. Peeters, and T. Tala, Nucl. Fusion **49**, 047001 (2009).
[7] A. V. Nedospasov, Phys. Plasmas **16**, 060501 (2009).
[8] H. M. Mott-Smith and I. Langmuir, Phys. Rev. **28**, 727 (1926).
[9] J. D. Swift and M. J. R. Schwar, *Electrical Probes for Plasma Diagnostics* (Elsevier, New York, 1970).
[10] *Low Temperature Plasmas* edited by R. Hippler, S. Pfau, M. Schmidt, and K. H. Schoenbach (Wiley-VCH, Berlin, 2008).
[11] K. Matsumoto and M. Sato, J. Appl. Phys. **54**, 1781 (1983).
[12] L. Oksuz, F. Soberón, and A. R. Ellingboe, J. Appl. Phys. **99**, 013304 (2006).
[13] A. D. Pajdarová, J. Vlček, P. Kudláček, and J. Lukáš, Plasma Sources Sci. Technol. **18**, 025008 (2009).
[14] R. H. Huddlestone, *Plasma Diagnostic Techniques*, edited by F. F. Chen (Academic, New York, 1965).
[15] I. H. Hutchinson, *Principles of Plasma Diagnostics* (Cambridge University Press, Cambridge, 2002).
[16] N. Hershkowitz, *Plasma Diagnostics* (Academic, San Diego, 1989) Vol. 1, pp. 113–183.
[17] B. E. Cherrington, Plasma Chem. Plasma Process. **2**, 113 (1982).
[18] L. Schott, in *Plasma Diagnostics*, edited by W. Lochte-Holtgreven (North-Holland, Amsterdam, 1968), pp. 668–731.
[19] J. W. Bradley, H. Bäcker, P. J. Kelly, and R. D. Arnell, Surf. Coat. Technol. **142–144**, 337 (2001).
[20] S. A. Nikiforov, G.-H. Kim, and G. -H. Rim, IEEE Trans. Plasma Sci. **31**, 94 (2003).
[21] A. C. Calder and J. G. Laframboise, Phys. Fluids B **2**, 655 (1990).
[22] C. H. Shih and E. Levi, AIAA J. **10**, 104 (1972).
[23] M. A. Lieberman, J. Appl. Phys. **66**, 2926 (1989).
[24] H. J. Oskam, R. W. Carlson, and T. Okuda, Physica (Amsterdam) **30**, 375 (1964).
[25] L. Loeb, *Recent Advances in Basic Processes of Gaseous Electronics* (University of California Press, Berkeley, 1973).
[26] J. C. McMahon, G. Z. Xu, and J. G. Laframboise, Phys. Plasmas **12**, 062109 (2005).
[27] P. M. Chunc, L. Talbot, and K. J. Touryan, AIAA J. **12**, 133 (1974).
[28] P. C. Stangeby, Phys. Fluids **27**, 2699 (1984).
[29] W. R. Hoegy and L. E. Wharton, J. Appl. Phys. **44**, 5365 (1973).
[30] P. C. Stangeby, Phys. Fluids **27**, 682 (1984).
[31] T. E. Sheridan and J. Goree, Phys. Rev. E **50**, 2991 (1994).
[32] P. C. Stangeby, *The Plasma Boundary of Magnetic Fusion Devices*, 1st ed. (Taylor & Francis, London, 2000), p. 41.
[33] F. F. Chen, *Introduction to Plasma Physics and Controlled Fusion*, 2nd ed. (Plenum, New York, 1984), p. 40.
[34] A. V. Nedospasov and D. A. Uzdensky, Contrib. Plasma Phys. **34**, 478 (1994).
[35] T. Okuda, R. W. Carlson, and H. J. Oskam, Physica (Amsterdam) **30**, 193 (1964).
[36] F. W. Crawford and R. Grard, J. Appl. Phys. **37**, 180 (1966).
[37] S.-B. Wang and A. E. Wendt, IEEE Trans. Plasma Sci. **27**, 1358 (1999).
[38] L. H. Brace, in *Measurement Techniques in Space Plasma, Particles*, edited by R. F. Pfaff, J. E. Borovsky, and D. T. Young (American Geophysical Union, Washington, D.C., 1998), pp. 23–34.
[39] G. Chiodini, C. Riccardi, and M. Fontanesi, Rev. Sci. Instrum. **70**, 2681 (1999).
[40] R. B. Lobbia and A. D. Gallimore, "High-speed dual Langmuir probe," Rev. Sci. Instrum. (submitted).